

Atg16L1, an essential factor for canonical autophagy, participates in hormone secretion from PC12 cells independently of autophagic activity

Koutaro Ishibashi^a, Takefumi Uemura^b, Satoshi Waguri^b, and Mitsunori Fukuda^a

^aDepartment of Developmental Biology and Neurosciences, Graduate School of Life Sciences, Tohoku University, Aobayama, Aoba-ku, Sendai, Miyagi 980-8578, Japan; ^bDepartment of Anatomy and Histology, Fukushima Medical University School of Medicine, Fukushima 960-1295, Japan

ABSTRACT Autophagy is a bulk degradation system in all eukaryotic cells and regulates a variety of biological activities in higher eukaryotes. Recently involvement of autophagy in the regulation of the secretory pathway has also been reported, but the molecular mechanism linking autophagy with the secretory pathway remains largely unknown. Here we show that Atg16L1, an essential protein for canonical autophagy, is localized on hormone-containing dense-core vesicles in neuroendocrine PC12 cells and that knockdown of Atg16L1 causes a dramatic reduction in the level of hormone secretion independently of autophagic activity. We also find that Atg16L1 interacts with the small GTPase Rab33A and that this interaction is required for the dense-core vesicle localization of Atg16L1 in PC12 cells. Our findings indicate that Atg16L1 regulates not only autophagy in all cell types, but also secretion from dense-core vesicles, presumably by acting as a Rab33A effector, in particular cell types.

Monitoring Editor

Thomas F.J. Martin
University of Wisconsin

Received: Jan 9, 2012

Revised: Jun 18, 2012

Accepted: Jun 21, 2012

INTRODUCTION

Autophagy is an intracellular bulk degradation process for proteins and organelles in all eukaryotic cells. Macroautophagy, the major type of autophagy (simply referred to as autophagy hereafter), is induced particularly when cells are exposed to nutrient-deprived conditions, and it is achieved by de novo formation of a double-membrane vesicle called the autophagosome and its subsequent fusion with lysosomes (reviewed in Levine and Klionsky, 2004; Nakatogawa *et al.*, 2009; Mizushima *et al.*, 2011). During the past decade, autophagy has been shown to be used for many aspects of cellular

events besides nutrient supply, including defense against bacterial intrusion, antigen presentation, removal of aggregated proteins, and quality control of organelles, and thus dysfunction of autophagy leads to a variety of human diseases, including cancer, neurodegeneration, and microbial infections (Mizushima *et al.*, 2008).

More recently, considerable attention has been paid to the relationship between autophagy and the secretory pathway because of the following observations. First, a genome-wide association study of ileal Crohn disease indicated that *ATG16L1*, which encodes a protein essential for canonical autophagy (Mizushima *et al.*, 2003), is a candidate for the gene responsible for susceptibility to human Crohn disease, a complex inflammatory disease involving the small intestine (Hampe *et al.*, 2007; Rioux *et al.*, 2007). Moreover, Atg16L1-deficient mice exhibit similar pathology in intestine (Cadwell *et al.*, 2008; Saitoh *et al.*, 2008), and the granule exocytotic pathway in Paneth cells (specialized secretory cells in the epithelium of the small intestine) is impaired in Atg16L1-deficient mice, implicating a role of autophagy in that particular secretory pathway. Second, it has recently been reported that autophagic proteins (or autophagic activity) play pivotal roles in the secretory pathway for extracellular delivery of interleukin (IL) 1 β and for osteoclastic bone resorption (Deselm *et al.*, 2011; Dupont *et al.*, 2011). However, whether autophagy

This article was published online ahead of print in MBoC in Press (<http://www.molbiolcell.org/cgi/doi/10.1091/mbc.E12-01-0010>) on June 27, 2012.

Address correspondence to: Mitsunori Fukuda (nori@m.tohoku.ac.jp).

Abbreviations used: EGFP, enhanced green fluorescent protein; GST, glutathione S-transferase; HBSS, Hank's balanced salt solution; HRP, horseradish peroxidase; LC3, microtubule-associated protein 1 light chain 3; MEF, mouse embryonic fibroblasts; mStr, monomeric Strawberry; NGF, nerve growth factor; NPY, neuropeptide Y; shRNA, short hairpin RNA; Syt I, synaptotagmin I; ULK1, Unc-51-like kinase 1.

© 2012 Ishibashi *et al.* This article is distributed by The American Society for Cell Biology under license from the author(s). Two months after publication it is available to the public under an Attribution–Noncommercial–Share Alike 3.0 Unported Creative Commons License (<http://creativecommons.org/licenses/by-nc-sa/3.0>). "ASCB," "The American Society for Cell Biology," and "Molecular Biology of the Cell" are registered trademarks of The American Society of Cell Biology.

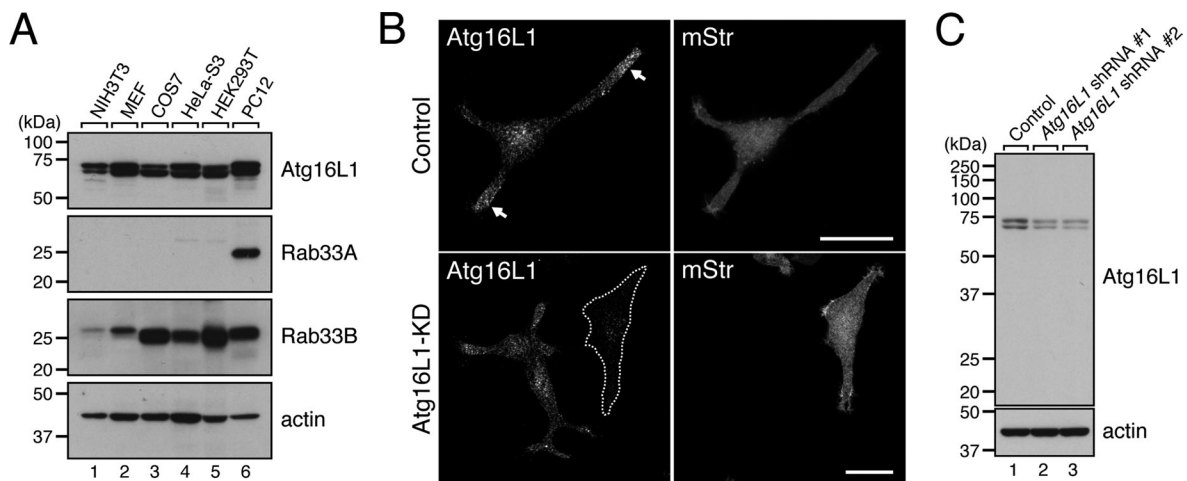


FIGURE 1: Endogenous Atg16L1 protein in PC12 cells is localized in the neurites. (A) Total lysates of various cell lines indicated were subjected to 10% SDS-PAGE followed by immunoblotting with anti-Atg16L1 antibody (top), anti-Rab33A antibody (second from top), anti-Rab33B antibody (third from top), and anti-actin antibody (bottom). Note that expression of Rab33A was restricted to PC12 cells (lane 6), whereas both Atg16L1 and Rab33B were expressed in all cell lines tested. (B) Unique localization of Atg16L1 in the neurites of PC12 cells. PC12 cells were cotransfected with *Atg16L1* shRNA (or control shRNA) and pmStr-C1 vector as a transfection marker and then immunostained with a specific antibody against Atg16L1 (see C). Note that the Atg16L1 signals were strongly concentrated in the neurites (top left, arrows) and that these signals did not appear after knockdown (KD) of Atg16L1 with *Atg16L1* shRNA #1 (an Atg16L1-KD cell is outlined in a broken line; bottom). Scale bars, 20 μ m. (C) Specificity of anti-Atg16L1 antibody as revealed by immunoblotting. The anti-Atg16L1 antibody specifically recognized doublet bands of Atg16L1 (lane 1), which correspond to the α and β forms of Atg16L1 (Mizushima *et al.*, 2003; Ishibashi *et al.*, 2011), and these signals were clearly attenuated by treatment with two independent *Atg16L1* shRNAs (lanes 2 and 3). PC12 cells were transfected with *Atg16L1* shRNA #1 or *Atg16L1* shRNA #2 and then cultured for 5 d. The cells were solubilized with 1% Triton X-100, and their lysates were subjected to 10% SDS-PAGE followed by immunoblotting with anti-Atg16L1 antibody (top) and anti-actin antibody (bottom). The size of the molecular mass markers (in kDa) is shown at the left.

directly regulates the secretory pathway remains unknown because the molecular mechanism by which autophagic proteins, especially Atg16L1, regulate the secretory pathway is poorly understood.

We previously found that Atg16L1 specifically interacts with two Rab33 isoforms, Rab33A and Rab33B (Itoh *et al.*, 2008), both of which are members of the Rab-type small GTPase family, which regulates a variety of membrane-trafficking events, including secretion (Fukuda, 2008; Stenmark, 2009), and interaction between Rab33B and Atg16L1 has been shown to modulate autophagic activity (Itoh *et al.*, 2008, 2011). Nevertheless, there have been no reports on either the functional significance of the interaction between Rab33A and Atg16L1 or the role of Rab33A in membrane traffic.

In this study, we unexpectedly discovered that Atg16L1 is localized on dense-core vesicles together with Rab33A in PC12 cells independently of autophagic activity. We were also able to show that knockdown of endogenous Atg16L1 protein in PC12 cells strongly inhibited hormone secretion, whereas suppression of canonical autophagy has no effect on hormone secretion at all. On the basis of our findings, we discuss the novel function of Atg16L1 as a Rab33A effector that regulates hormone secretion in PC12 cells.

RESULTS

Atg16L1 protein is localized in the neurites of PC12 cells independently of autophagic activity

To determine the functional relationship between Rab33A and Atg16L1, we first investigated the expression of Rab33A, Rab33B, and Atg16L1 in a variety of mammalian cell lines by immunoblotting with specific antibodies. Consistent with the fact that autophagy occurs in every cell type, expression of Atg16L1 and its ligand Rab33B was found in all the cell lines tested. Rab33A, on the other hand,

was specifically expressed in PC12 cells, cells that were originally derived from a pheochromocytoma in the adrenal medulla of a rat and that have often been used as a secretion model (Tsuboi and Fukuda, 2006; Figure 1A, lane 6). Similarly, abundant expression of *Rab33A* mRNA restricted to the brain (e.g., human cerebellum) and B lymphoblasts has been reported in the BioGPS database (available at <http://biogps.org>). We therefore focused on PC12 cells to analyze the relationship between Rab33A and Atg16L1 and investigated the subcellular localization of Atg16L1 in nerve growth factor (NGF)-differentiated PC12 cells by immunofluorescence analysis. To our surprise, strong Atg16L1 signals were observed in the neurites (especially the distal part of the neurites) of PC12 cells even under nutrient-rich conditions (Figure 1B, top left, arrows). This unique localization of Atg16L1 in PC12 cells was in sharp contrast to its localization in mouse embryonic fibroblasts (MEFs) and NIH 3T3 cells, in which Atg16L1 signals were observed as scattered dots, that is, isolation membranes, precursor structures of autophagosomes, in the cytoplasm, especially under starved conditions (Mizushima *et al.*, 2003; Itoh *et al.*, 2008). The Atg16L1 signals observed in PC12 cells cannot have been attributable to nonspecific interaction with the antibody because immunoblotting showed that the anti-Atg16L1 antibody used in this study specifically recognizes two forms of Atg16L1 (Atg16L1 α , 63 kDa; and Atg16L1 β , 71 kDa) in PC12 cells (Figure 1C, lane 1) and because small interfering RNA (siRNA)-mediated knockdown of endogenous Atg16L1 protein clearly caused failure of the Atg16L1 immunostaining signals to appear (Figure 1B, bottom; see also Figure 1C, lanes 2 and 3, showing that Atg16L1 band intensity was clearly decreased after Atg16L1 knockdown). We therefore concluded that endogenous Atg16L1 protein is actually concentrated in the neurites of PC12 cells.

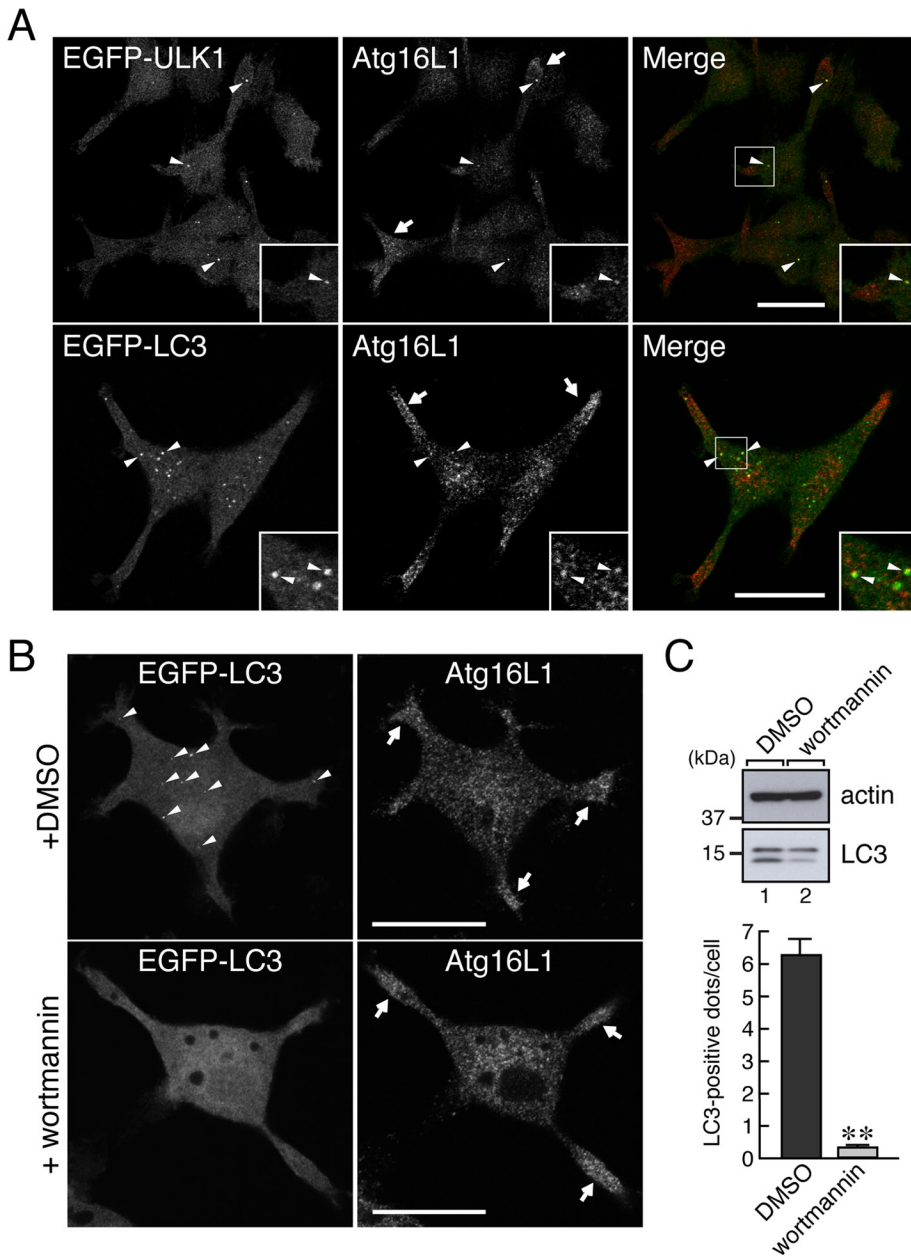


FIGURE 2: Localization of Atg16L1 protein in the neurites of PC12 cells is independent of autophagic activity. (A) Atg16L1 signals in the neurites of PC12 cells differed from the signals of autophagy-related organelles (isolation membranes and autophagosomes). PC12 cells stably expressing EGFP-ULK1 (an isolation membrane marker; green) or EGFP-LC3 (an autophagosome marker; green) under starved conditions were immunostained with anti-Atg16L1 antibody (red). Note that Atg16L1 signals in the neurites (top and bottom, arrows) were negative for both EGFP-ULK1 and EGFP-LC3, whereas some Atg16L1 dots in the cell body colocalized with EGFP-ULK1 dots and EGFP-LC3 dots (arrowheads in the insets). Insets, magnified views of the boxed area. Scale bars, 20 μm. (B) Atg16L1 signals in the neurites of PC12 cells were insensitive to wortmannin treatment. PC12 cells stably expressing EGFP-LC3 were starved for 30 min in HBSS in the presence of dimethyl sulfoxide or 100 nM wortmannin, fixed with 4% paraformaldehyde, and then immunostained with anti-Atg16L1 antibody. Note that, in contrast to the control cells (top left, arrowheads), the Atg16L1 signals in the neurites persisted even under autophagy-defective conditions (bottom right, arrows), where hardly any EGFP-LC3-positive dots were observed (bottom left). Scale bars, 20 μm. (C) Inhibition of canonical autophagy by wortmannin. Top, PC12 cells were treated for 30 min with HBSS containing 100 nM wortmannin. After solubilizing the cells with 1% Triton X-100, we analyzed total cell lysates by 15% SDS-PAGE followed by immunoblotting with anti-actin antibody and anti-LC3 antibody. Bottom, PC12 cells stably expressing EGFP-LC3 were incubated for 30 min with HBSS containing 100 nM wortmannin (or dimethyl sulfoxide [DMSO] alone), and then the

To determine whether the Atg16L1 signals observed in the neurites simply correspond to the isolation membranes and/or autophagosomes, we compared the Atg16L1 signals with a known isolation membrane marker (Unc-51-like kinase 1 [ULK1]) and autophagosome marker (microtubule-associated protein 1 light chain 3 [LC3]). As shown in Figure 2A, all of the scattered enhanced green fluorescent protein (EGFP)-ULK1 dots were colocalized with Atg16L1-positive dots (arrowheads, top), and no colocalization was observed in the distal part of the neurites, where Atg16L1 signals were abundant (arrows, top). Similarly, some scattered EGFP-LC3 dots were partially colocalized with Atg16L1-positive dots in the cell body (Figure 2A, bottom, arrowheads), and they were rarely present in the neurites (Figure 2A, bottom, arrows). Moreover, the Atg16L1 signals in the neurites were clearly insensitive to treatment with 100 nM wortmannin (Figure 2B, right, arrows), a phosphatidylinositol 3-kinase inhibitor that blocks autophagy, that is, inhibition of LC3 lipidation (Figure 2C, the lower band of LC3, lane 2) and reduction in the number of EGFP-LC3 puncta (Figure 2B, bottom left, and Figure 2C, bottom). These results allowed us to conclude that the Atg16L1 signals in the neurites of PC12 cells are not related to autophagic activity.

Atg16L1 protein is localized on dense-core vesicles in PC12 cells

Next we attempted to identify the organelles where Atg16L1 protein is localized in the neurites. Because dense-core vesicles are known to be concentrated in the neurites of PC12 cells (Fukuda *et al.*, 2002b), we costained the cells with the anti-Atg16L1 antibody and antibodies to two dense-core vesicle markers (synaptotagmin [Syt] I and Rab3). As anticipated, endogenous Atg16L1 protein was highly colocalized with Syt I on the dense-core vesicles in the neurites of PC12 cells, and partial colocalization between Atg16L1 and Rab3 was also observed (Figure 3A). The association between endogenous Atg16L1 protein and dense-core vesicles was confirmed by immunoaffinity purification of dense-core vesicles (Figure 3B).

EGFP-LC3 dots in the cells ($n > 70$) were counted as described previously (Itoh *et al.*, 2008, 2011). Under these experimental conditions, there was a marked decrease in the lipidated form of LC3 (LC3-II; a marker for autophagy; lane 2, lower band in the LC3 panel) and in LC3-dot formation (lower graph). ** $p < 0.01$ (Student's unpaired t test).

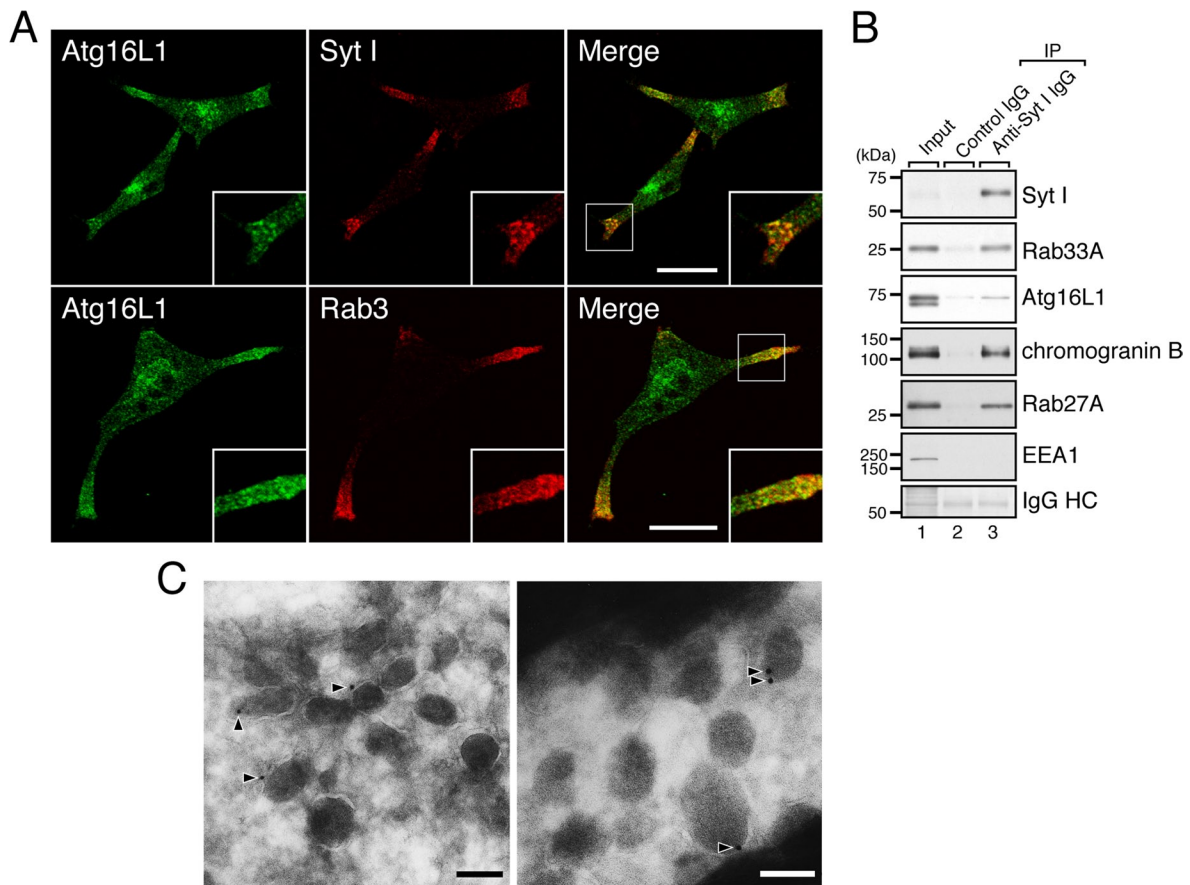


FIGURE 3: Atg16L1 is localized on dense-core vesicles in the neurites of PC12 cells. (A) PC12 cells were coimmunostained with anti-Atg16L1 antibody and anti-Syt I antibody or anti-Rab3 antibody. Atg16L1 signals in the distal portion of the neurites were colocalized with two dense-core vesicle markers—Syt I (top) and Rab3 (bottom). Insets, magnified views of the boxed area. Scale bars, 20 μ m. (B) Localization of endogenous Atg16L1 protein and Rab33A protein on dense-core vesicles as revealed by immunoaffinity purification of dense-core vesicles. Dense-core vesicles were immunoprecipitated from PC12 cells by using anti-Syt I antibody as described in *Materials and Methods*. The dense-core vesicle fraction was subjected to 10% SDS-PAGE followed by immunoblotting with the antibodies indicated. The amount of immunoglobulin heavy chain (IgG HC) used for immunoprecipitation was determined by amido black staining of the blots (bottom). Under our experimental conditions, only Atg16L1 β was copurified with the dense-core vesicles, despite the fact both the Atg16L1 α and Atg16L1 β isoforms had interacted with Rab33A in the coimmunoprecipitation assays (see Figure 4A). We speculate the reason for this is that Atg16L1 α binds Rab33A less effectively than Atg16L1 β does and that Atg16L1 is released from the Rab33A on dense-core vesicles during the vigorous washing procedures using a vortex. The size of the molecular mass markers (in kDa) is shown at the left. (C) Localization of endogenous Atg16L1 protein on dense-core vesicles as revealed by immuno-electron microscopy. PC12 cells were cultured under normal nutrient-rich conditions and then fixed with 4% paraformaldehyde + 0.1% glutaraldehyde, and ultrathin cryosections were cut and immunolabeled with anti-Atg16L1 antibody followed by incubation with secondary antibody conjugated with colloidal gold particles (12 nm). Note that the gold particles—that is, the anti-Atg16L1 antibody molecules—were clearly associated with the surface of dense-core vesicles (arrowheads). Bars, 100 nm.

Moreover, immuno-electron microscopic analyses with the specific antibody clearly demonstrated the presence of Atg16L1 protein on dense-core vesicles (Figure 3C, arrowheads).

Rab33A recruits Atg16L1 to dense-core vesicles in PC12 cells

Because Atg16L1 is able to interact with Rab33A *in vitro* (Itoh *et al.*, 2008) and Rab33A is localized on dense-core vesicles in PC12 cells (Tsuboi and Fukuda, 2006), we hypothesized that Atg16L1 is recruited to Rab33A-positive dense-core vesicles in PC12 cells. To verify our hypothesis, we investigated the endogenous interaction between Rab33A and Atg16L1 in PC12 cells by performing a coimmunopre-

cipitation assay with the anti-Rab33A-specific antibody. The results showed that Atg16L1 efficiently coimmunoprecipitated with Rab33A (Figure 4A, middle, lane 3). Of interest, Atg12-conjugated Atg5, which interacts with Atg16L1, was also copurified with Rab33A (Figure 4A, bottom, lane 3), a finding that was consistent with the fact that Atg16L1 forms a complex with Atg12–5 in the cytosol (Mizushima *et al.*, 2003). To our surprise, no interaction between Atg16L1 and Rab33B was detected in PC12 cells by coimmunoprecipitation assays with two different anti-Rab33B-specific antibodies (Supplemental Figure S1A, lanes 4 and 5). We do not know the reason for this finding, but we speculate that the level of expression of Rab33A in PC12 cells may be much higher than the level of expression of Rab33B in

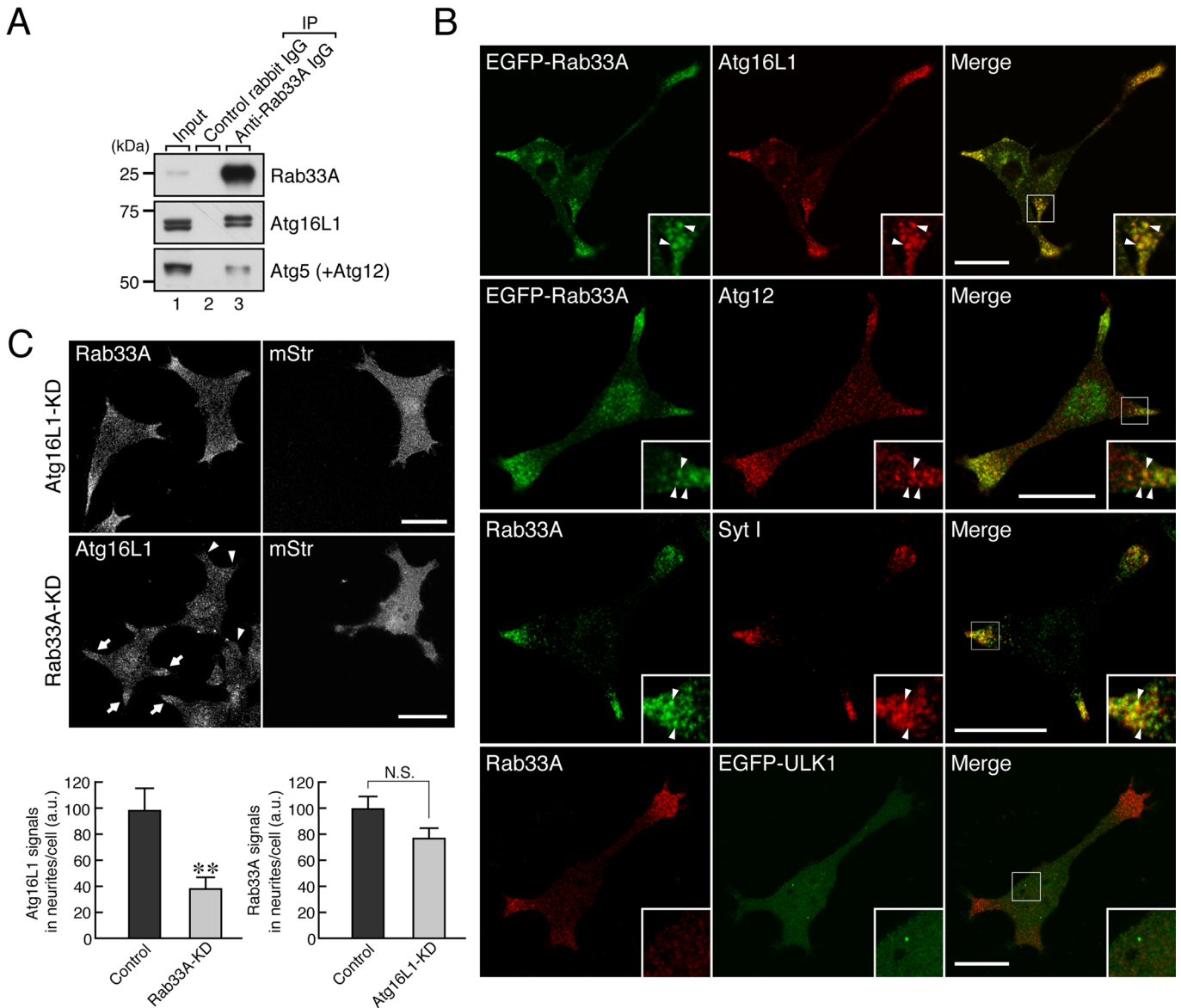


FIGURE 4: Rab33A recruits Atg16L1 to dense-core vesicles in PC12 cells. (A) Atg16L1 interacts with Rab33A, a dense-core vesicle-resident Rab. Coimmunoprecipitation assays were performed as described in *Materials and Methods*. Protein A-Sepharose beads coupled with anti-Rab33A IgG or control rabbit IgG were incubated with PC12 cell lysates. Total cell lysates (input; lane 1) and the proteins bound to the beads (lane 3) were analyzed by 10% SDS-PAGE followed by immunoblotting with anti-Rab33A antibody (top), anti-Atg16L1 antibody (middle), and anti-Atg5 antibody (bottom). Note that both isoforms of Atg16L1 were coimmunoprecipitated with Rab33A (compare middle, lanes 2 and 3), although Atg16L1 α seemed to bind Rab33A less efficiently (see also Figure 3B). The size of the molecular mass markers (in kDa) is shown at the left. (B) Rab33A is colocalized with Atg16L1 in the neurites of PC12 cells. EGFP-Rab33A was colocalized with endogenous Atg16L1 protein ($67.1 \pm 2.8\%$ colocalization in neurites; $n = 6$) and Atg12 protein in the neurites of PC12 cells (top and second row). Endogenous Rab33A protein was also colocalized with Syt I (a dense-core vesicle marker; third row; $60.2 \pm 4.3\%$ colocalization in neurites; $n = 11$), the same as endogenous Atg16L1 protein was, whereas endogenous Rab33A protein was not colocalized with EGFP-ULK1 (an isolation membrane marker; bottom row). Insets, magnified views of the boxed area. Arrowheads indicate the colocalized dots. Scale bars, 20 μ m. (C) Rab33A is required for the dense-core vesicle localization of Atg16L1 in PC12 cells. PC12 cells were cotransfected with Rab33A shRNA (or Atg16L1 shRNA) and pmStr-C1 vector as a transfection marker and then immunostained with anti-Rab33A antibody or anti-Atg16L1 antibody. Note that the clear reduction in Atg16L1 signals in the neurites as a result of Rab33A knockdown (middle) in comparison with the signals of untransfected PC12 cells (arrows). By contrast, the Rab33A signals in the neurites were unaltered by the Atg16L1 knockdown (top), indicating that Rab33A recruits Atg16L1 to dense-core vesicles. Scale bars, 20 μ m. The graphs at the bottom show quantification of Rab33A signals and Atg16L1 signals in the neurites in the images above ($n > 40$). a.u., arbitrary units. ** $p < 0.01$ (Student's unpaired t test); N.S., not significant.

PC12 cells. Alternatively, the two anti-Rab33B antibodies used for the coimmunoprecipitation assays may simply inhibit the endogenous interaction between Atg16L1 and Rab33B.

Consistent with the results of the coimmunoprecipitation assays, EGFP-Rab33A was colocalized with Atg16L1 (and also with Atg12) in the neurites of PC12 cells (Figure 4B, top row and second row).

Furthermore, since endogenous Rab33A protein was colocalized with Syt I, a dense-core vesicle marker (Figure 4B, third row) and did not exhibit any colocalization with the isolation membrane marker EGFP-ULK1 (Figure 4B, bottom; see also Supplemental Figure S1B), a Rab33A–Atg16L1 complex is likely to be specifically present on dense-core vesicles rather than on isolation membranes. If Rab33A functions as a scaffold to recruit Atg16L1 to dense-core vesicles, knockdown of Rab33A should result in failure of Atg16L1 signals to appear on dense-core vesicles. As anticipated, knockdown of endogenous Rab33A protein in PC12 cells by specific short hairpin RNA (shRNA) caused a significant reduction in the Atg16L1 signals in the neurites (Figure 4C, middle, arrowheads, and bottom left, graph). By contrast, knockdown of endogenous Atg16L1 protein in PC12 cells by specific shRNA had no effect on the dense-core vesicle localization of Rab33A (Figure 4C, top) or on Rab33A signals (Figure 4C, bottom right, graph). We therefore concluded that Atg16L1 is localized on dense-core vesicles in PC12 cells as a result of a specific interaction with Rab33A.

Atg16L1 regulates hormone secretion independently of autophagic activity

Finally, we performed neuropeptide Y (NPY) secretion assays to determine whether Atg16L1 is actually involved in the secretion pathway of dense-core vesicles. Peptide hormone NPY fused with T7-tagged glutathione S-transferase (GST), which targets dense-core vesicles (Fukuda *et al.*, 2002a), was transiently expressed in PC12 cells together with Atg16L1 shRNA or control shRNA. The cells were then stimulated with low-KCl buffer or high-KCl buffer, and the amount of NPY-T7-GST secreted into the extracellular space from the dense-core vesicles was measured as described in *Materials and Methods*. Of interest, both low-KCl-dependent NPY secretion (basal/constitutive secretion pathway) and high-KCl-dependent NPY secretion (regulated secretion pathway) were found to be dramatically decreased in the Atg16L1-knockdown PC12 cells (Figure 5A). Such effects were unlikely to be off-target effects of shRNAs because we obtained the same results with two independent Atg16L1 shRNAs (#1 and #2). Furthermore, since the total level of NPY-T7-GST expression in control cells and in Atg16L1-knockdown cells did not differ too much (Figure 5A, inset), the decreased NPY-T7-GST secretion from the Atg16L1-knockdown cells is unlikely to be attributable to the decreased number of dense-core vesicles. Actually, knockdown of Atg16L1 had little or no effect on the expression of several proteins involved in hormone secretion and of dense-core vesicle-associated proteins (Supplemental Figure S2, A and B) or on the transport of dense-core vesicles to the neurites (Supplemental Figure S2C). Of interest, however, only the total level of expression of chromogranin B, a dense-core vesicle cargo protein, was clearly decreased in Atg16L1-knockdown PC12 cells (Supplemental Figure S2, A and B), although chromogranin B was normally localized in the neurites of even the Atg16L1-knockdown PC12 cells (Supplemental Figure S2C, bottom row).

Because knockdown of Atg16L1 also caused inhibition of canonical autophagy in MEFs (Ishibashi *et al.*, 2011), the possibility remained that inhibition of autophagy itself results in the decreased hormone secretion, and to rule out this possibility, we also performed NPY secretion assays under several autophagy-defective conditions. When PC12 cells were treated with 100 nM wortmannin for 30 min before the secretion assay, neither NPY-T7-GST secretion nor the total level of NPY-T7-GST expression was altered (Supplemental Figure S3C). Similarly, the amount of NPY-T7-GST secreted from PC12 cells expressing the Atg4B C74A (CA) mutant

or ULK1 kinase-dead mutant, both of which inhibit canonical autophagy (Fujita *et al.*, 2008b; Hara *et al.*, 2008; Supplemental Figure S3A), was comparable to the amount of NPY-T7-GST secreted from control PC12 cells (Supplemental Figure S3B). Moreover, both Atg13-knockdown PC12 cells and ULK1-knockdown PC12 cells exhibited normal hormone secretion activity (Figure 5B). These results, together with the fact that Atg16L1 protein is associated with dense-core vesicles in neurites (Figure 3), indicated that Atg16L1 regulates secretion of NPY independently of its autophagic activity.

Because Rab33A is required for the dense-core vesicle localization of Atg16L1 in PC12 cells (Figure 4C), we investigated the effect of Rab33A knockdown on NPY secretion. As anticipated, knockdown of Rab33A by two independent Rab33A shRNAs in PC12 cells attenuated both low-KCl-dependent and high-KCl-dependent NPY-T7-GST secretion, the same as Atg16L1 knockdown did (Figure 5C), strongly suggesting that the Rab33A–Atg16L1 complex regulates the hormone secretion pathway.

DISCUSSION

In the present study, we used neuroendocrine PC12 cells to investigate the involvement of autophagic factors in hormone secretion and found that Atg16L1, an essential factor for canonical autophagy, has a novel secretory function in PC12 cells, presumably by acting as a Rab33A effector. Atg16L1 is localized on Rab33A-positive dense-core vesicles in the neurites of PC12 cells independently of their autophagic activity (Figures 1–4) and is required for hormone (NPY) secretion (Figure 5A). Because knockdown of either Atg16L1 or Rab33A attenuated both low-KCl-dependent and high-KCl-dependent NPY secretion (Figure 5, A and C), the Rab33A–Atg16L1 complex is likely to regulate both constitutive and regulated hormone secretion pathways. Secretory pathways generally consist of a number of steps, including vesicle formation, maturation, transport along the cytoskeleton, tethering/docking, priming, and fusion with the plasma membrane, and we speculate that Atg16L1 is involved in several steps in the secretory pathway. First, Atg16L1 is partly involved in biogenesis of dense-core vesicles, because the total amount of chromogranin B, which was originally believed to be essential for biogenesis of dense-core vesicles, was decreased in Atg16L1 (or Rab33A)-knockdown PC12 cells (Supplemental Figures S2, A and B, and S5B). However, since other dense-core vesicle marker proteins—for example, Syt I and Rab3—are normally expressed and localized in the neurites of even Atg16L1-knockdown PC12 cells (Supplemental Figure S2, A–C), the total number of dense-core vesicles may be less affected. Actually, recent studies on chromogranin B knockout (or chromogranin A/B double knockout) mice revealed that chromogranin B is not essential for dense-core vesicle biogenesis and that it regulates peptide hormone secretion (Obermüller *et al.*, 2010; Díaz-Vera *et al.*, 2012). Consistent with the results of these studies, our preliminary data indicated the presence of morphologically mature dense-core vesicles in Atg16L1-knockdown PC12 cells at the electron microscopic level (unpublished data). Thus Atg16L1 is also likely to be involved in a late step(s) in the secretory pathway, presumably downstream of a transport step, because knockdown of Atg16L1 had little effect on dense-core vesicle formation (Supplemental Figure S2, A and B) or on the transport of dense-core vesicles to the neurites (Supplemental Figure S2C). In any event, extensive research will be necessary to determine the exact step(s) in the secretory pathway in which Atg16L1 is involved and whether deficiency of chromogranin B is involved in the reduced hormone secretion activity of Atg16L1-knockdown PC12 cells.

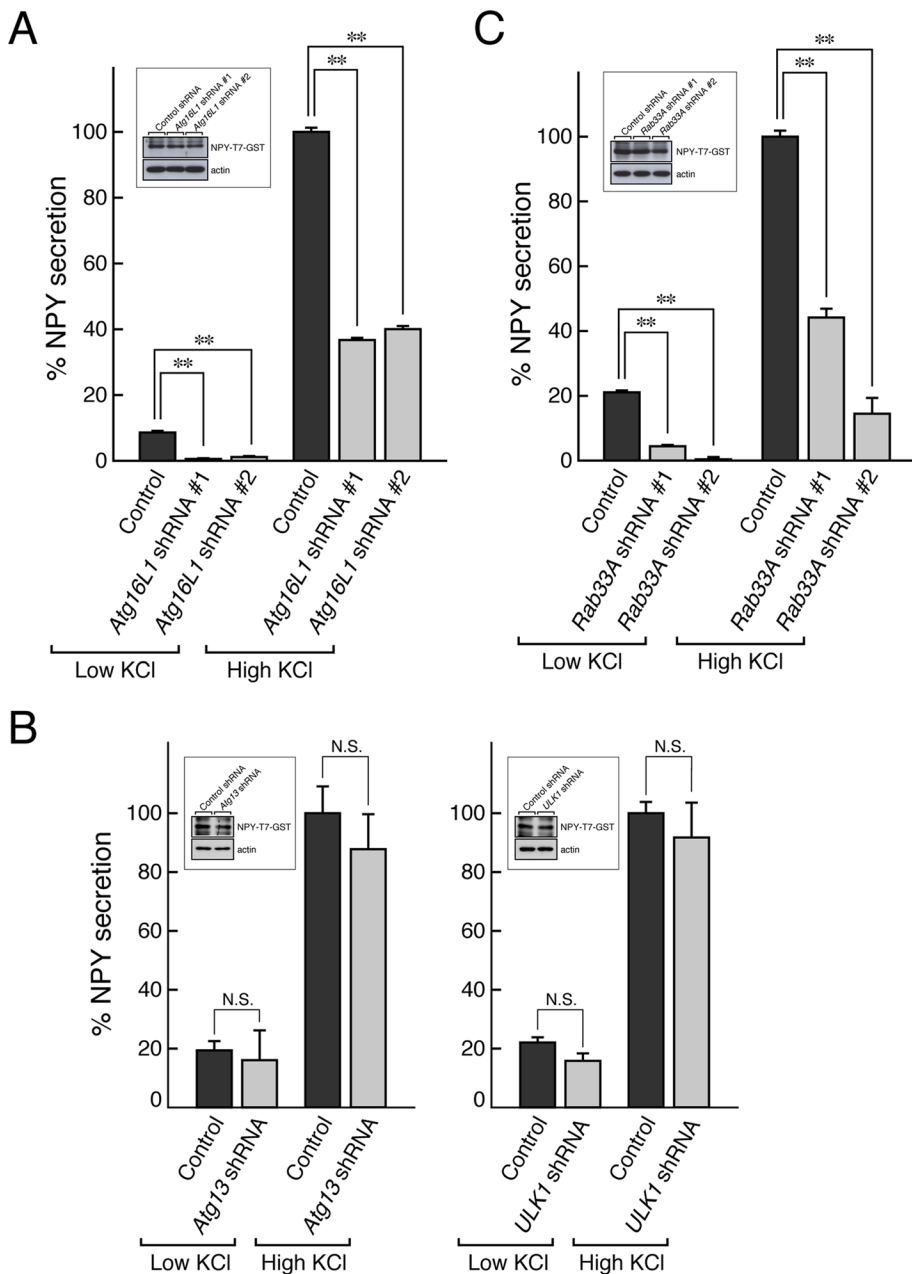


FIGURE 5: Atg16L1 regulates hormone secretion in PC12 cells independently of their autophagic activity. (A) Effect of Atg16L1 knockdown on hormone secretion from PC12 cells. NPY-T7-GST secretion assays were performed as described in *Materials and Methods*. The results are expressed as percentages of high-KCl-dependent NPY secretion from control PC12 cells. Bars indicate the means and SE of three determinations. Note that Atg16L1 knockdown resulted in a dramatic reduction in both low-KCl- and high-KCl-dependent NPY secretion (shaded bars) in comparison with the control PC12 cells (closed bars). ** $p < 0.01$ (Student's unpaired t test). Under our experimental conditions, knockdown of Atg16L1 had little effect on the total amount of hormone (NPY-T7-GST; inset), although the total amount of NPY-T7-GST in Atg16L1 shRNA #2-expressing cells was somewhat decreased. Total cell lysates of PC12 cells that had been cotransfected with pShooter-NPY-T7-GST and pSilencer-Atg16L1 (or control empty pSilencer vector) were subjected to 10% SDS-PAGE followed by immunoblotting with anti-T7 tag antibody and anti-actin antibody. The knockdown efficacy of Atg16L1 shRNAs is shown in Figure 1C. (B) Effect of Atg13 knockdown or ULK1 knockdown on hormone secretion from PC12 cells. NPY-T7-GST secretion assays were performed as described. N.S., not significant in comparison with the control cells. Note that neither Atg13 knockdown nor ULK1 knockdown affected hormone secretion but that knockdown of each of them significantly inhibited starvation-induced autophagy (Supplemental Figure S5A). Total cell lysates of PC12 cells that had been cotransfected with pShooter-NPY-T7-GST and pSilencer-Atg13 (pSilencer-ULK1 or control empty pSilencer vector) were subjected to 10% SDS-PAGE followed by

Because autophagic activity is believed to be involved in other secretory pathways (Cadwell *et al.*, 2009; Deselm *et al.*, 2011; Dupont *et al.*, 2011), the most important finding in this study is that the secretory function of Atg16L1 is independent of its function in autophagy (Figure 2B and Supplemental Figure S3). The secretory function of Atg16L1 is unlikely to be common to all cell types, and it may be limited to certain cell types that specifically express Rab33A, which is required for the secretory vesicle localization of Atg16L1 (Figures 1A and 4C). Because Rab33A has been reported to be abundantly expressed at the mRNA level in the brain, lymphocytic system, and hematopoietic system (Jacobsen *et al.*, 2005; and the BioGPS database), we speculate that Atg16L1 regulates certain secretory events in the brain and these systems together with Rab33A. Because these events occur in macrophage-related cells and have recently been shown to be related to autophagy (Deselm *et al.*, 2011; Dupont *et al.*, 2011), it will be very interesting to investigate the involvement of Rab33A in IL-1 β secretion and osteoclastic bone resorption. The relation between Rab33A and Crohn disease may also be worth investigating because a recent finding indicates that Atg16L1 is differently involved in canonical autophagy and Crohn disease caused by a defective secretory pathway (Fujita *et al.*, 2009). Because deficiency of Atg5 (an Atg16L1-binding protein) and of Atg7 (an E1 enzyme that

immunoblotting with anti-T7 tag antibody and anti-actin antibody (inset). Under our experimental conditions, inhibition of autophagy had little effect on the total amount of NPY-T7-GST. (C) Effect of Rab33A knockdown on hormone secretion from PC12 cells. Rab33A shRNA was transiently coexpressed with NPY-T7-GST in PC12 cells. The NPY-T7-GST secretion assays were performed as described in A. Note that Rab33A knockdown caused inhibition of both the low-KCl-dependent and high-KCl-dependent NPY secretion (shaded bars). ** $p < 0.01$ (Student's unpaired t test). Total cell lysates of PC12 cells that had been cotransfected with pShooter-NPY-T7-GST and pSilencer-Rab33A (or control empty pSilencer vector) were subjected to 10% SDS-PAGE followed by immunoblotting with anti-T7 tag antibody and anti-actin antibody. Under our experimental conditions, knockdown of Rab33A had little effect on the total amount of hormone (NPY-T7-GST; inset), although the total amount of NPY-T7-GST in Rab33A shRNA #2-expressing cells was somewhat decreased. The results shown are representative of at least two independent experiments.

activates Atg12 so that it conjugates with Atg5) also resulted in a similar Crohn disease phenotype (Cadwell *et al.*, 2009) and Rab33 is able to bind both isolated Atg16L1 and the Atg12–5–16L1 complex (Itoh *et al.*, 2008), it is tempting to speculate that the Atg12–5–16L1 complex functions as a Rab33A effector in the regulation of particular secretion events. Consistent with our speculation, knockdown of endogenous Atg5 protein in PC12 cells caused inhibition of hormone secretion (Supplemental Figure S4C). Furthermore, overexpression of Atg16L1 alone in PC12 cells weakly but significantly inhibited hormone secretion (Supplemental Figure S4B), whereas overexpression of a Rab33A-binding-deficient mutant Atg16L1- Δ 201-214 (Ishibashi *et al.*, 2011), which was unable to target dense-core vesicles (Supplemental Figure S4A), in PC12 cells had no effect on hormone secretion (Supplemental Figure S4B). These observations also supported our hypothesis that Rab33A functions together with the Atg12–5–16L1 complex during hormone secretion. A free Atg16L1 molecule may act as a dominant-negative construct that traps Rab33A (i.e., an inappropriate complex between Rab33A and Atg16L1 alone may inhibit hormone secretion). A similar dominant-negative effect of Atg16L1 on canonical autophagy was reported when Atg16L1 alone was expressed in MEFs (Fujita *et al.*, 2008a). Although the Atg12–5–16L1 complex has recently been shown to have E3-like enzyme activity toward LC3 (Hanada *et al.*, 2007; Fujita *et al.*, 2008a), since no LC3 signals were observed on dense-core vesicles (Figure 2A, bottom), the Atg12–5–16L1 complex together with Rab33A may have additional function other than E3-like activity during hormone secretion.

In summary, we reported the first evidence that Atg16L1 together with Rab33A on dense-core vesicles regulates hormone secretion from PC12 cells independently of autophagic activity. Our discovery of the involvement of Rab33A–Atg16L1 complex in hormone secretion from PC12 cells should provide clues to elucidating the relationship between autophagy and secretion in other systems.

MATERIALS AND METHODS

Materials

Anti-Rab3 mouse monoclonal antibody, anti-Munc18 mouse monoclonal antibody, and anti-chromogranin B mouse monoclonal antibody were obtained from BD Transduction Laboratories (Lexington, KY). Anti-Syt I (SYA-148) mouse monoclonal antibody and anti-Syt I luminal domain rabbit polyclonal antibody were purchased from StressGen Biotechnologies (Victoria, Canada) and Synaptic Systems (Göttingen, Germany), respectively. Anti-Atg12 (or Apg12) rabbit polyclonal antibody was from Invitrogen (Carlsbad, CA). Anti-Rab33B mouse monoclonal antibody (D5) was from Frontier Science (Ishikari, Japan). Anti-syntaxin-1 mouse monoclonal antibody (HPC1) and anti-VAMP2 rabbit polyclonal antibody were from Santa Cruz Biotechnology (Santa Cruz, CA) and Wako Pure Chemical Industries (Osaka, Japan), respectively. Anti- β -actin (G043) mouse monoclonal antibody was from Applied Biological Materials (Richmond, Canada). Anti-Atg16L1 rabbit polyclonal antibody, anti-Rab27A rabbit polyclonal antibody, anti-Rab33A rabbit polyclonal antibody, and anti-Rab33B rabbit polyclonal antibody were prepared as described previously (Saegusa *et al.*, 2006; Itoh *et al.*, 2008; Ishibashi *et al.*, 2011), and their specificity in PC12 cells was confirmed by immunoblotting (Figure 1C and Supplemental Figure S1A). Anti-Atg5 rabbit polyclonal antibody was produced by using purified GST-mouse Atg5 as the antigen (Itoh *et al.*, 2008), and it was affinity purified as described previously (Fukuda and Mikoshiba, 1999). Horseradish peroxidase (HRP)-conjugated anti-T7 tag mouse monoclonal antibody and anti-hemagglutinin (HA) tag mouse monoclonal antibody were from Merck Biosciences Novagen (Darmstadt, Germany) and Roche Molecular

Biochemicals (Mannheim, Germany), respectively. HRP-conjugated anti-mouse/rabbit immunoglobulin G (IgG) and HRP-conjugated protein A were obtained from SouthernBiotech (Birmingham, AL) and GE Healthcare (Little Chalfont, United Kingdom), respectively. The fluorescent dye-conjugated secondary antibodies (Alexa Fluor 488-, 594-, and 633-labeled anti-mouse/rabbit IgGs) were from Invitrogen. All other reagents used in this study were analytical grade or the highest grade commercially available.

Plasmid construction

pEGFP-C1-Atg16L1- Δ 201-214 and pEF-T7-Atg16L1- Δ 201-214 were produced by conventional PCR techniques using a following oligonucleotide with a *Bst*XI site (underlined): 5'-ACCAGATGGATG-GCTGAGAAGGCCCAAAGGCGTCAAGCACGGCTGCAG-3'. pEGFP-C1-Rab33A, pmStrawberry (pmStr)-C1-Rab33A, and pEGFP-C1-Atg16L1 were prepared as described previously (Itoh *et al.*, 2008). The cDNAs of human ULK1, a ULK1 kinase-dead mutant (M92A; ULK1-KD), and a human Atg4B mutant (C74A; Atg4B-CA) were kindly provided by Tamotsu Yoshimori (Graduate School of Medicine, Osaka University, Osaka, Japan) and subcloned into the pEF-HA tag vector (Fukuda, 2002). The human ULK1 cDNA and mouse LC3 cDNA (Itoh *et al.*, 2011) were subcloned into the pMRX-IRES-puro-EGFP vector (Saitoh *et al.*, 2003). pSilencer 2.1-U6 neo vector (Ambion, Austin, TX), which encodes Atg16L1 shRNA (a 19-base target site: 5'-ACTGAGGAAACTACTGAG-3' for Atg16L1 shRNA #1 and 5'-CTGTTAGGGAAGATCACTG-3' for Atg16L1 shRNA #2), was constructed according to the manufacturer's notes (referred to as pSilencer-Atg16L1 #1 and #2, respectively). The knockdown efficiency of the plasmids was evaluated by expressing pSilencer-Atg16L1 #1 or #2 (or a control pSilencer vector) in PC12 cells (Figure 1C). Rab33A shRNA expression vectors (a 19-base target site: 5'-ATCCCTCTTGTACCGTGAT-3' for Rab33A shRNA #1 and 5'-TGTGCATGCAGTGGTCTTT-3' for Rab33A shRNA #2), Atg5 shRNA expression vectors (a 19-base target site: 5'-TTGGCCTACT-GTTCGATCT-3' for Atg5 shRNA #1 and 5'-CTGTTTACAGTCAGCT-TAT-3' for Atg5 shRNA #2), an Atg13 shRNA expression vector (a 19-base target site: 5'-GAGAAGAATGTCCGAGAAT-3'), and a ULK1 shRNA expression vector (a 19-base target site: 5'-AGACTCCTGT-GACACAGAT-3') were similarly produced (see also Tsuboi and Fukuda, 2006; Ganley *et al.*, 2009; Florey *et al.*, 2011). The effect of shRNAs against Rab33A (#2), Atg16L1 (#1), Atg5 (#2), Atg13, and ULK1 on starvation-induced autophagy was also evaluated by LC3-dot formation in PC12 cells (Supplemental Figure S5A). Modified siRNA duplexes (stealth RNA) against mouse/rat Atg16L1 and a nontargeting scramble sequence (control stealth RNA) were obtained from Invitrogen (MSS293862 and 12935-113, respectively).

Cell culture, transfection, and infection

PC12 cells were cultured at 37°C in DMEM containing 10% horse serum, 10% fetal bovine serum, and antibiotics with or without nerve growth factor (100 ng/ml; Merck, Darmstadt, Germany) under a 5% CO₂ atmosphere. Plasmids were transfected into PC12 cells by using Lipofectamine 2000 (Invitrogen) according to the manufacturer's notes. Starvation was achieved by washing the cells once with Hank's balanced salt solution (HBSS; Sigma-Aldrich, St. Louis, MO). Inhibition of autophagy was achieved by exposing the cells to wortmannin (Merck Biosciences Calbiochem, Darmstadt, Germany), an inhibitor of phosphatidylinositol 3-kinases, at a concentration of 100 nM for 30 min. The EGFP-LC3-positive dots were counted as described previously (Itoh *et al.*, 2008, 2011). Retrovirus infection and Plat-E cell culture were performed as described previously (Morita *et al.*, 2000). To obtain stable cell lines, PC12 cells infected with retrovirus

expressing EGFP-ULK1 or EGFP-LC3 were selected with 4 $\mu\text{g}/\text{ml}$ puromycin (Merck Biosciences Calbiochem).

Immunostaining

PC12 cells were cultured at 37°C in DMEM containing 10% horse serum and 10% fetal bovine serum on poly-L-lysine-coated 35-mm dishes under 5% CO₂. One microgram of each plasmid of interest was transfected into PC12 cells by using Lipofectamine 2000 according to the manufacturer's notes. At 36–48 h after transfection, the cells were treated with 100 ng/ml NGF, and 1 d later the cells were incubated in HBSS for 1.5 h. The cells were then fixed with 4% paraformaldehyde (Merck Biosciences Calbiochem) for 20 min, permeabilized with 0.3% Triton X-100 for 2 min, and blocked with the blocking buffer (1% bovine serum albumin and 0.1% Triton X-100 in phosphate-buffered saline) for 1 h. The cells were immunostained with anti-Atg16L1 antibody, anti-Syt I antibody, anti-Rab3 antibody, anti-Rab33A antibody, and/or anti-chromogranin B antibody, followed by Alexa Fluor 488- and/or 594-labeled secondary IgG. The cells were examined for fluorescence with a confocal laser-scanning microscope (FluoView 1000; Olympus, Tokyo, Japan), and the images were processed with Photoshop software, version CS4 (Adobe, San Jose, CA). Immunofluorescence signals were quantified with MetaMorph software (Molecular Devices, Sunnyvale, CA), and a colocalization analysis was performed with ImageJ software, version 1.42q (National Institutes of Health, Bethesda, MD). The data were expressed as means and SEs.

Electron microscopy analysis

PC12 cells were cultured under normal nutrient-rich conditions and then fixed with 4% paraformaldehyde–0.1% glutaraldehyde in phosphate buffer (pH 7.4). Ultrathin cryosections were cut and immunolabeled with anti-Atg16L1 antibody, followed by incubation with secondary antibody conjugated with colloidal gold particles (12 nm). The procedures used for cell freezing, sectioning, and the immunoreactions have been described previously (Waguri and Komatsu, 2009). The sections were viewed with an electron microscope (JEM1200; JEOL, Peabody, MA).

Immunoprecipitation and immunoaffinity purification of dense-core vesicles

Protein A–Sepharose beads (GE Healthcare) coupled with anti-Rab33A IgG (or control rabbit IgG) were incubated for 1 h in PC12 cell lysates solubilized with 1% Triton X-100. After washing of the beads three times, the proteins bound to the beads were analyzed by 10% SDS–PAGE, followed by immunoblotting with anti-Rab33A antibody, anti-Atg16L1 antibody, and anti-Atg5 antibody. Immunoreactive bands were visualized with HRP-conjugated protein A and detected by enhanced chemiluminescence (GE Healthcare). Immunoaffinity purification of Syt I-bound dense-core vesicles with anti-Syt I IgG-conjugated magnetic beads was performed as described previously with modifications (Fukuda, 2004). In brief, PC12 cells (two 10-cm dishes; 90% confluent) were placed in 1 ml of 50 mM 4-(2-hydroxyethyl)-1-piperazineethanesulfonic acid (HEPES)–KOH, pH 7.2, 150 mM NaCl, 1 mM MgCl₂, 1 mM dithiothreitol, and appropriate protease inhibitors (homogenization buffer) and homogenized by passing the cells through 2.5-ml syringe with 27-gauge needle. After centrifugation at 800 \times g for 5 min, the supernatant obtained was incubated for 1 h at 4°C with anti-Syt I antibody or control mouse IgG (~1 μg) and then for 1 h at 4°C with Dynabeads M-280 (Invitrogen). The beads were washed vigorously with the homogenization buffer by using a vortex, and the washing was repeated four or five times. The dense-core vesicle fraction was analyzed as

described by 10% SDS–PAGE, followed by immunoblotting with the antibodies indicated in Figure 3B and Supplemental Figure S2B.

NPY secretion assays

NPY-T7-GST secretion assays in PC12 cells were performed as described previously (Fukuda *et al.*, 2002a; Fukuda and Kanno, 2005). In brief, PC12 cells (6-cm dish) were cotransfected with 1 μg of pShooter-NPY-T7-GST and 2 μg of each plasmid of interest by using Lipofectamine 2000 according to the manufacturer's notes. Three days after transfection, cells were washed with prewarmed, low-KCl buffer (5.6 mM KCl, 145 mM NaCl, 2.2 mM CaCl₂, 0.5 mM MgCl₂, 5.6 mM glucose, and 15 mM HEPES-KOH at pH 7.4) and then stimulated for 20 min at 37°C with either low-KCl buffer or high-KCl buffer (56 mM KCl, 95 mM NaCl, 2.2 mM CaCl₂, 0.5 mM MgCl₂, 5.6 mM glucose, and 15 mM HEPES-KOH at pH 7.4). Released NPY-T7-GST was recovered by incubation with glutathione–Sepharose beads (GE Healthcare) and analyzed by immunoblotting with HRP-conjugated anti-T7 tag antibody. The intensity of the immunoreactive bands on x-ray film was quantified with YabGellImageX software (version 1.2; freely available at <https://sites.google.com/site/yabgel/home>) and normalized by the amount of expressed NPY-T7-GST in total cell lysates. Total cell lysates were obtained by incubation with a lysis buffer (10 mM Tris-HCl at pH 8.0, 150 mM NaCl, 1 mM EDTA, and 1% NP-40, and appropriate protease inhibitors).

ACKNOWLEDGMENTS

We thank Tamotsu Yoshimori for donating Atg4B-CA, ULK1, and ULK1-KD cDNAs; Toshio Kitamura for Plat-E cells and retroviral vectors; Shoji Yamaoka for pMRX-IRES-puro vectors; Atsuko Yabashi and Katsuyuki Kanno for technical help in electron microscopy; Megumi Aizawa, Ayaka Yatsu, Takahide Matsui, and Takashi Itoh for technical assistance; and members of the Fukuda laboratory for valuable discussions. This work was supported in part by Grants-in-Aid for Scientific Research from the Ministry of Education, Culture, Sports, and Technology of Japan (to M.F.) and by a grant from the Global COE Program (Basic and Translational Research Center for Global Brain Science) of the Ministry of Education, Culture, Sports, and Technology of Japan (to M.F.). K.I. was supported by the Japan Society for the Promotion of Science.

REFERENCES

- Cadwell K *et al.* (2008). A key role for autophagy and the autophagy gene *Atg16l1* in mouse and human intestinal Paneth cells. *Nature* 456, 259–263.
- Cadwell K, Patel KK, Komatsu M, Virgin HW, Stappenbeck TS (2009). A common role for Atg16L1, Atg5 and Atg7 in small intestinal Paneth cells and Crohn disease. *Autophagy* 5, 250–252.
- Deselm CJ *et al.* (2011). Autophagy proteins regulate the secretory component of osteoclastic bone resorption. *Dev Cell* 21, 966–974.
- Díaz-Vera J, Camacho M, Machado JD, Domínguez N, Montesinos MS, Hernández-Fernaud JR, Luján R, Borges R (2012). Chromogranins A and B are key proteins in amine accumulation, but the catecholamine secretory pathway is conserved without them. *FASEB J* 26, 430–438.
- Dupont N, Jiang S, Pilli M, Ornatowski W, Bhattacharya D, Deretic V (2011). Autophagy-based unconventional secretory pathway for extracellular delivery of IL-1 β . *EMBO J* 30, 4701–4711.
- Florey O, Kim SE, Sandoval CP, Haynes CM, Overholtzer M (2011). Autophagy machinery mediates macroendocytic processing and entotic cell death by targeting single membranes. *Nat Cell Biol* 13, 1335–1343.
- Fujita N, Hayashi-Nishino M, Fukumoto H, Omori H, Yamamoto A, Noda T, Yoshimori T (2008b). An Atg4B mutant hampers the lipidation of LC3 paralogs and causes defects in autophagosome closure. *Mol Biol Cell* 19, 4651–4659.
- Fujita N, Itoh T, Omori H, Fukuda M, Noda T, Yoshimori T (2008a). The Atg16L complex specifies the site of LC3 lipidation for membrane biogenesis in autophagy. *Mol Biol Cell* 19, 2092–2100.

- Fujita N, Saitoh T, Kageyama S, Akira S, Noda T, Yoshimori T (2009). Differential involvement of Atg16L1 in Crohn disease and canonical autophagy: analysis of the organization of the Atg16L1 complex in fibroblasts. *J Biol Chem* 284, 32602–32609.
- Fukuda M (2002). Synaptotagmin-like protein (Slp) homology domain 1 of Slac2-a/melanophilin is a critical determinant of GTP-dependent specific binding to Rab27A. *J Biol Chem* 277, 40118–40124.
- Fukuda M (2004). RNA interference-mediated silencing of synaptotagmin IX, but not synaptotagmin I, inhibits dense-core vesicle exocytosis in PC12 cells. *Biochem J* 380, 875–879.
- Fukuda M (2008). Regulation of secretory vesicle traffic by Rab small GTPases. *Cell Mol Life Sci* 65, 2801–2813.
- Fukuda M, Kanno E (2005). Analysis of the role of Rab27 effector Slp4-a/granuphilin-a in dense-core vesicle exocytosis. *Methods Enzymol* 403, 445–457.
- Fukuda M, Kanno E, Saegusa C, Ogata Y, Kuroda TS (2002b). Slp4-a/granuphilin-a regulates dense-core vesicle exocytosis in PC12 cells. *J Biol Chem* 277, 39673–39678.
- Fukuda M, Katayama E, Mikoshiba K (2002a). The calcium-binding loops of the tandem C2 domains of synaptotagmin VII cooperatively mediate calcium-dependent oligomerization. *J Biol Chem* 277, 29315–29320.
- Fukuda M, Mikoshiba K (1999). A novel alternatively spliced variant of synaptotagmin VI lacking a transmembrane domain: implications for distinct functions of the two isoforms. *J Biol Chem* 274, 31428–31434.
- Ganley IG, Lam du H, Wang J, Ding X, Chen S, Jiang X (2009). ULK1-ATG13-FIP200 complex mediates mTOR signaling and is essential for autophagy. *J Biol Chem* 284, 12297–12305.
- Hampe J *et al.* (2007). A genome-wide association scan of nonsynonymous SNPs identifies a susceptibility variant for Crohn disease in *ATG16L1*. *Nat Genet* 39, 207–211.
- Hanada T, Noda NN, Satomi Y, Ichimura Y, Fujioka Y, Takao T, Inagaki F, Ohsumi Y (2007). The Atg12-Atg5 conjugate has a novel E3-like activity for protein lipidation in autophagy. *J Biol Chem* 282, 37298–37302.
- Hara T, Takamura A, Kishi C, Iemura S, Natsume T, Guan JL, Mizushima N (2008). FIP200, a ULK-interacting protein, is required for autophagosome formation in mammalian cells. *J Cell Biol* 181, 497–510.
- Ishibashi K, Fujita N, Kanno E, Omori H, Yoshimori T, Itoh T, Fukuda M (2011). Atg16L2, a novel isoform of mammalian Atg16L that is not essential for canonical autophagy despite forming an Atg12–5–16L2 complex. *Autophagy* 7, 1500–1513.
- Itoh T, Fujita N, Kanno E, Yamamoto A, Yoshimori T, Fukuda M (2008). Golgi-resident small GTPase Rab33B interacts with Atg16L and modulates autophagosome formation. *Mol Biol Cell* 19, 2916–2925.
- Itoh T, Kanno E, Uemura T, Waguri S, Fukuda M (2011). OATL1, a novel autophagosome-resident Rab33B-GAP, regulates autophagosomal maturation. *J Cell Biol* 192, 839–853.
- Jacobsen M, Reipsilber D, Gutschmidt A, Neher A, Feldmann K, Mollenkopf HJ, Ziegler A, Kaufmann SHE (2005). Ras-associated small GTPase 33A, a novel T cell factor, is down-regulated in patients with tuberculosis. *J Infect Dis* 192, 1211–1218.
- Levine B, Klionsky DJ (2004). Development by self-digestion: molecular mechanisms and biological functions of autophagy. *Dev Cell* 6, 463–477.
- Mizushima N, Kuma A, Kobayashi Y, Yamamoto A, Matsubae M, Takao T, Natsume T, Ohsumi Y, Yoshimori T (2003). Mouse Apg16L, a novel WD-repeat protein, targets to the autophagic isolation membrane with the Apg12-Apg5 conjugate. *J Cell Sci* 116, 1679–1688.
- Mizushima N, Levine B, Cuervo AM, Klionsky DJ (2008). Autophagy fights disease through cellular self-digestion. *Nature* 451, 1069–1075.
- Mizushima N, Yoshimori T, Ohsumi Y (2011). The role of atg proteins in autophagosome formation. *Annu Rev Cell Dev Biol* 27, 107–132.
- Morita S, Kojima T, Kitamura T (2000). Plat-E: an efficient and stable system for transient packaging of retroviruses. *Gene Ther* 7, 1063–1066.
- Nakatogawa H, Suzuki K, Kamada Y, Ohsumi Y (2009). Dynamics and diversity in autophagy mechanisms: lessons from yeast. *Nat Rev Mol Cell Biol* 10, 458–467.
- Obermüller S *et al.* (2010). Defective secretion of islet hormones in chromogranin-B deficient mice. *PLoS One* 5, e8936.
- Rioux JD *et al.* (2007). Genome-wide association study identifies new susceptibility loci for Crohn disease and implicates autophagy in disease pathogenesis. *Nat Genet* 39, 596–604.
- Saegusa C, Tanaka T, Tani S, Itohara S, Mikoshiba K, Fukuda M (2006). Decreased basal mucus secretion by Slp2-a-deficient gastric surface mucous cells. *Genes Cells* 11, 623–631.
- Saitoh T *et al.* (2008). Loss of the autophagy protein Atg16L1 enhances endotoxin-induced IL-1 β production. *Nature* 456, 264–268.
- Saitoh T, Nakayama M, Nakano H, Yagita H, Yamamoto N, Yamaoka S (2003). TWEAK induces NF- κ B p100 processing and long lasting NF- κ B activation. *J Biol Chem* 278, 36005–36012.
- Stenmark H (2009). Rab GTPases as coordinators of vesicle traffic. *Nat Rev Mol Cell Biol* 10, 513–525.
- Tsuboi T, Fukuda M (2006). Rab3A and Rab27A cooperatively regulate the docking step of dense-core vesicle exocytosis in PC12 cells. *J Cell Sci* 119, 2196–2203.
- Waguri S, Komatsu M (2009). Biochemical and morphological detection of inclusion bodies in autophagy-deficient mice. *Methods Enzymol* 453, 181–196.